Nuclear Magnetic Resonance Spectroscopy of a ^{1}H-^{31}P Heteronuclear System in the Earth's Field: Spinor Properties and Demonstration of a Quantum Computing C-NOT Gate

Simon WW Manley

SimonWWManley@gmail.com

Abstract

Trimethyl phosphate provides a convenient heteronuclear system for experiments with low-cost Earth's Field NMR equipment, illustrating J-coupling and its application in NMR quantum computing. While only the ^{1}H signal is readily acquired, both the ^{1}H and ^{31}P nuclear spins can be manipulated independently by $\mathbf{B_1}$ pulses.

Introduction

Nuclear Magnetic Resonance in the Earth's Field (EF-NMR) provides a low-cost technique for demonstrating principles of nuclear spin in elementary physics classes. Commercial systems have been marketed (Teachspin Inc., Buffalo, NY), including MRI functionality (Callaghan, Eccles & Seymour, 1997), and designs published which are suitable for projects in the student practical laboratory (Michal, 2010) or home construction (Trevelyan, 2019).

With signal frequency around 2 kHz and linewidths of the order of 1 Hz, chemical shifts of parts per million cannot be resolved in EF-NMR, but J-couplings are prominent in heteronuclear systems, splitting spectral lines into easily-resolved doublets.

The sensitivity for signal acquisition by Faraday induction in NMR is approximately proportional to the 3rd power of the gyromagnetic ratio, γ, which determines the Larmor precession frequency, f, in a magnetic field, $\mathbf{B_0}$, according to $f = \mathbf{B_0}\gamma/2\pi$.

The following table shows the precession frequencies and relative sensitivities for common spin ½ nuclei at a typical value of the Earth's field, $\mathbf{B_0}$ = 50 μT.

Nucleus	$\gamma/2\pi$ (MHz/T)	f @ 50 μT (Hz)	Sensitivity (%)
^{1}H	42.576	2129	100.0
^{13}C	10.708	535	1.6
^{19}F	40.052	2003	83.3
^{31}P	17.235	862	6.6

Fluoro-carbon compounds, such as 1,4 difluorobenzene, have been used to demonstrate heteronuclear J-coupling, with the advantage that the precession frequencies of ^{1}H and ^{19}F lie close enough to fall within the bandwidth of typical EF-NMR amplifiers (Robinson *et al*, 2006; Mann *et al*, 2019). In the classroom environment, however, fluorobenzenes have the disadvantages of being toxic, volatile and hazardously flammable. Their expense is also significant, since ER-NMR must use specimen volumes of hundreds of milliliters. Compounds labelled with ^{13}C are also disqualified for classroom EF-NMR experiments by cost as well as low sensitivity.

Phosphorus compounds, such as the inexpensive industrial solvent trimethyl phosphate (TMP), contain the spin ½ species ^{31}P at near 100% isotopic abundance. TMP has

low volatility, low flammability and only moderate toxicity – favorable properties for health and safety in the classroom. Although its low sensitivity makes the ^{31}P signal difficult to detect in EF-NMR, it is easy to *manipulate* the ^{31}P spin in a ^{1}H-^{31}P heteronuclear system with $\mathbf{B_1}$ pulses at the calculated precession frequency, while monitoring only the signal from the ^{1}H spin.

In this paper, we report the EF-NMR properties of trimethyl phosphate, where 9 magnetically-equivalent ^{1}H spins are J-coupled through 3 covalent bonds to a single ^{31}P spin.

Equipment and Data Processing

Prior to application of $\mathbf{B_1}$ pulses and signal acquisition, samples of 300 ml water or trimethyl phosphate were pre-polarized for 6 seconds in a field of 25 mT (about 500 times the Earth's field), generated by a solenoid surrounding the receiver coil and specimen. The sketch below shows the layout of the coil system, inside a heavy (10 kg) aluminium screen which served to minimize interference by fields radiated from electrical mains wiring and appliances. $\mathbf{B_1}$ pulses of calibrated amplitude and duration were applied to the pre-polarization coil, which was then short-circuited during signal acquisition to provide additional shielding. Further details of physical layout, coil construction and electronic circuitry are provided in the Appendix.

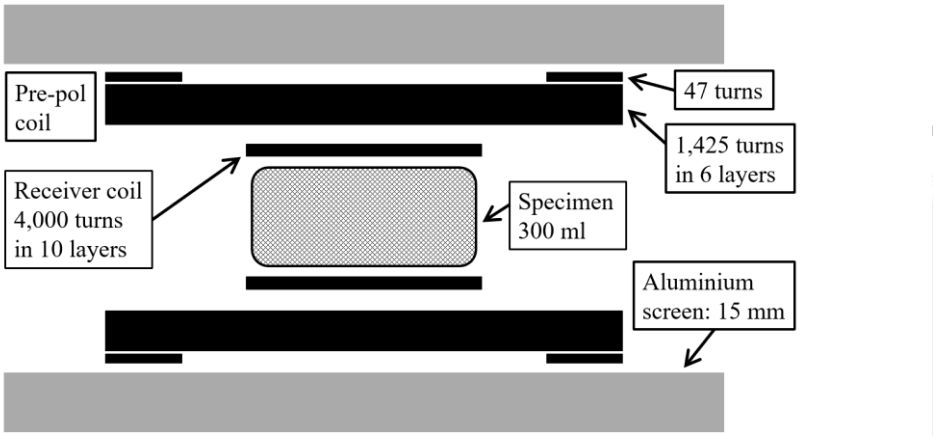

The Free Induction Decay signal (FID) and its Fourier transform were clearly recognizable in real time on a Digital Storage Oscilloscope (DSO). Signal-to-noise ratio improved with averaging over 16 sweeps.

To foster conceptual understanding in the classroom environment, data was processed in the familiar Microsoft Excel spreadsheet, using the Fast Fourier Transform (FFT) of the Data Analysis module to derive spectra. To maximize spectral resolution while keeping the spreadsheet to a manageable size, the signal frequency was shifted down from around 2,156 Hz to 156 Hz by heterodyning with a 2 kHz local oscillator. The product was acquired at 1,000 samples per second for 2 seconds using the 10-bit analog-to-digital function of an Arduino microcontroller. The 2,000 samples were then padded out to 4,096 entries with zeroes for analysis by the FFT, yielding a frequency bin width of 0.24 Hz. For display, the spectra were shifted back to the frequency of the original FID signal, around 2,156 Hz. Absorption mode Lorentzian functions were fitted by least squares.

^{1}H FID and Spectra of Water and Trimethyl Phosphate

The following images show the ^{1}H FID and spectra for water (top) and TMP (bottom). The heterodyne beats in the TMP signal, corresponding to the J-coupling split of 11 Hz in the spectral doublet, were immediately obvious in the real-time signal on the DSO. Offline

processing in Excel of FID signals averaged over 16 sweeps resulted in the spectra shown on the right. Note that frequency increases left-to-right, as in the conventions of physics (rather than the reverse which is used to display chemical shifts in analytical NMR).

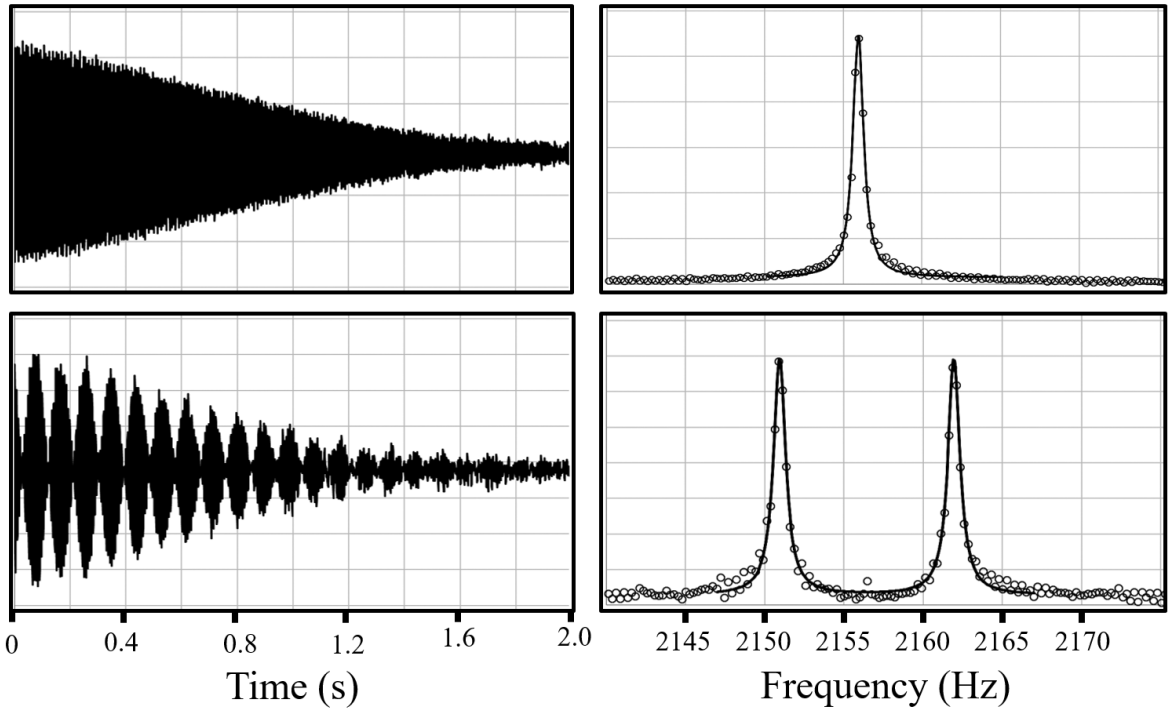

The amplitude of the recorded FID with a water specimen after a π/2 $\mathbf{B_1}$ pulse at the ^{1}H frequency was initially around 10 μV p-p, decaying smoothly over 2 seconds with an approximately exponential profile. The signal from TMP began at around 6 μV p-p, decaying a little more rapidly than the water signal, consistent with the effect of the higher viscosity on T_2, the time-constant for decay of the transverse magnetization.

The Fourier spectrum for water showed a single peak at 2156 Hz, while TMP presented a doublet split by J = 11 Hz. Diurnal variation in frequencies was within a range of 2 Hz, corresponding to fluctuations of around 50 nT in the Earth's magnetic field of about 50.6 μT at our mid-latitude location.

Tipping the ^{31}P Spins

Protons in the TMP molecule interact through J-coupling with a single ^{31}P nucleus, and hence show a doublet spectrum. The ^{31}P spin, however, interacts with 9 magnetically-equivalent protons, 3 in each of the 3 methyl groups. This is predicted to produce a complex spectrum for ^{31}P, with 10 lines, whose amplitude will vary according to the Pascal's triangle rule.

From the accurately-determined ^{1}H precession frequency, and published values for the gyromagnetic ratios of ^{1}H and ^{31}P, the center frequency of the ^{31}P spectrum was readily calculated, circa 872 Hz.

Although we do not record the ^{31}P signal, $\mathbf{B_1}$ pulses manipulating the ^{31}P spins should cover the range of frequencies involved. The graph following shows the calculated spectrum for ^{31}P, and the spectrum of the narrowest practicable $\mathbf{B_1}$ pulse, 15 ms duration, spanning only 13 cycles at the ^{31}P frequency. The difficulty is evident. The energy of the $\mathbf{B_1}$ pulse falls off at frequencies where the ^{31}P spectrum still has appreciable amplitude.

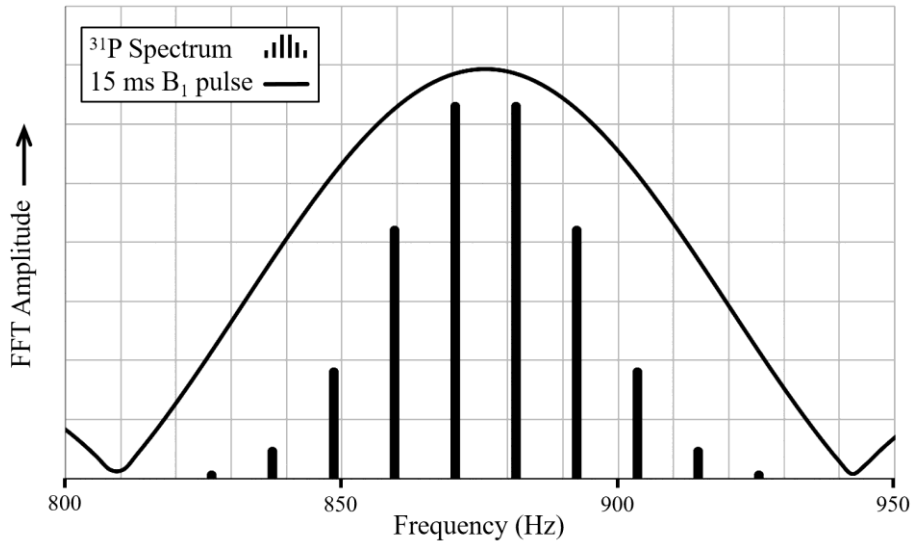

The bandwidth is insufficient to tip the entire population of ^{31}P spins through equal angles. Thus some loss of coherence is expected, particularly at larger tip angles. Despite this difficulty, data of adequate quality to demonstrate important teaching points could be obtained.

Calibrating the π/2 B_1 pulse for ^{31}P

We calibrated the π/2 pulse for ^{31}P using the method described as *inverse detection* in NMR textbooks. After an initial **B_1** pulse at the ^{1}H frequency and a time delay of 1/(2J), tipping the ^{31}P spins through an angle of exactly π/2 results in cancellation of the signal due to conversion of the transverse ^{1}H magnetization into antiphase quantum coherences.

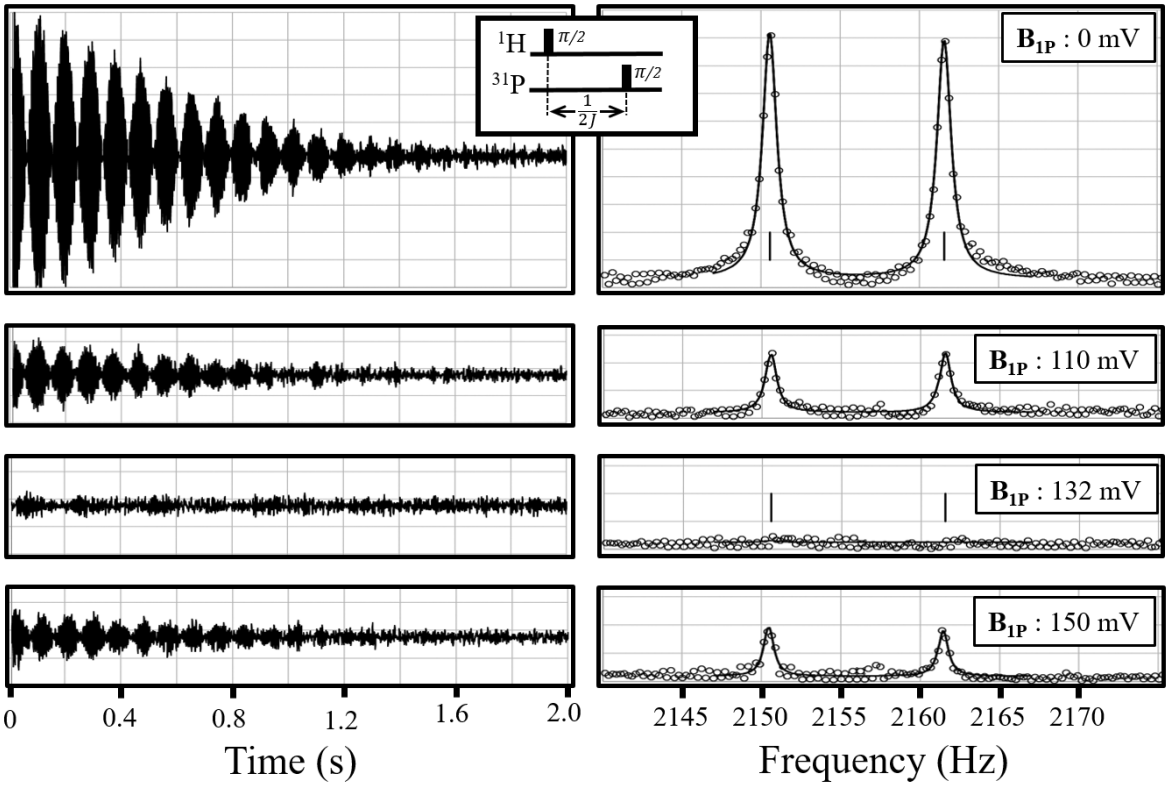

In the images above, the ^{1}H FID and spectra are displayed on the same scales for different amplitudes of a 15 ms **B_1** pulse at the ^{31}P precession frequency. It is apparent that the ^{1}H signal vanished at about 132 mV RMS.

Examining the first 20 samples of the FID revealed a reversal of the phase of the ^{1}H signal as the strength of the $\mathbf{B_1}$ pulse at the ^{31}P frequency was increased beyond the null value.

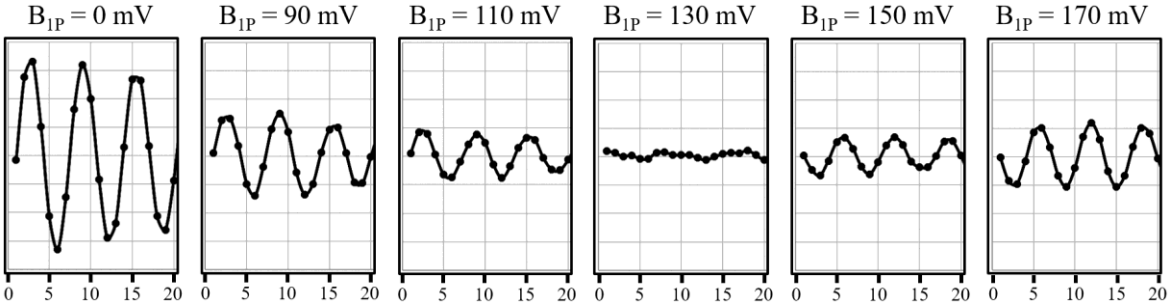

The phase reversal reveals the mechanism of the signal cancellation. The recorded ^{1}H signal after a $\mathbf{B_1}$ pulse at the ^{31}P frequency was the resultant of two components of opposite phases, which cancelled when exactly balanced (antiphase quantum coherence).

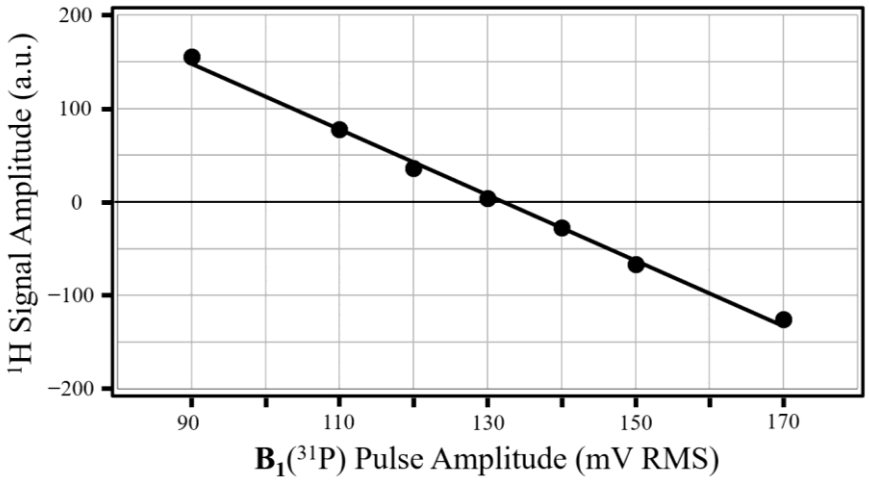

The relationship between the amplitude of the ^{1}H signal (measured as the sum of the peak values in the FFT spectrum corrected for the noise level) and the ^{31}P $\mathbf{B_1}$ pulse amplitude was approximately linear around the null value (graph above), when the amplitudes beyond the null were plotted as negative values, in accord with the phase of the FID signal. Estimating the π/2 pulse amplitude from such a plot was more convenient than laborious trial and error seeking the exact value at which the ^{1}H FID vanished.

Frequency Selective B_1 Pulses Split the ^{1}H Doublet

To excite only one line in a spectral doublet requires a $\mathbf{B_1}$ pulse whose energy is confined to a narrow range of frequencies. In NMR jargon, such frequency-selective pulses are termed *soft*, referring to their low amplitude and long duration. Achieving sufficient selectivity to split a spectral doublet is challenging in EF-NMR. The low frequency suggests pulses of impossibly long duration, and simple equipment permits only the setting of pulse duration rather than controlling the continuously varying amplitude of a shaped pulse.

The calculated spectrum of a rectangular pulse (image following) suggests a work-around for these difficulties. Deep nulls surround the central peak, separated by twice the reciprocal of the pulse duration.

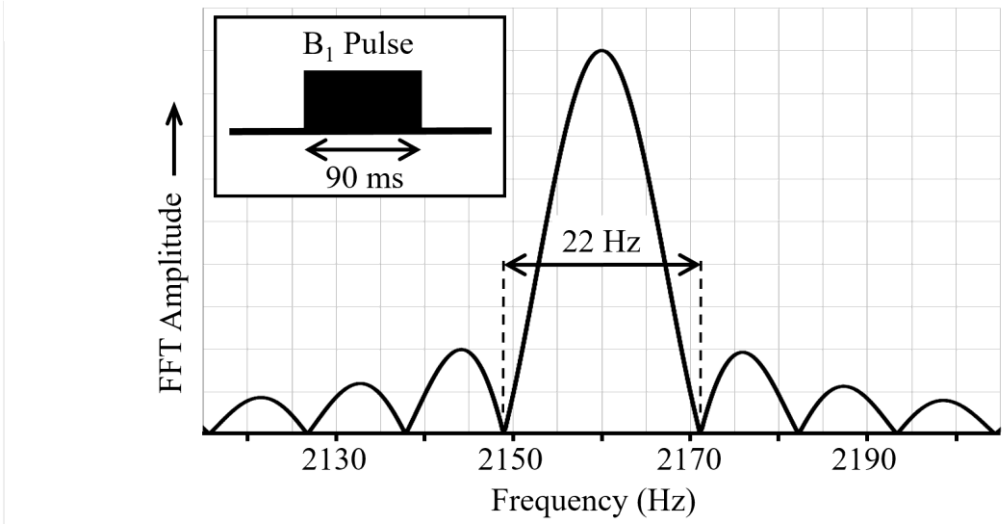

With a pulse duration of 1/J, and **B₁** frequency chosen to place one line of the 11 Hz doublet on the spectral peak, the other line fell on a null. By careful adjustment of the **B₁** frequency in steps of 0.25 Hz, a single line in the ^{1}H spectrum of TMP could be isolated.

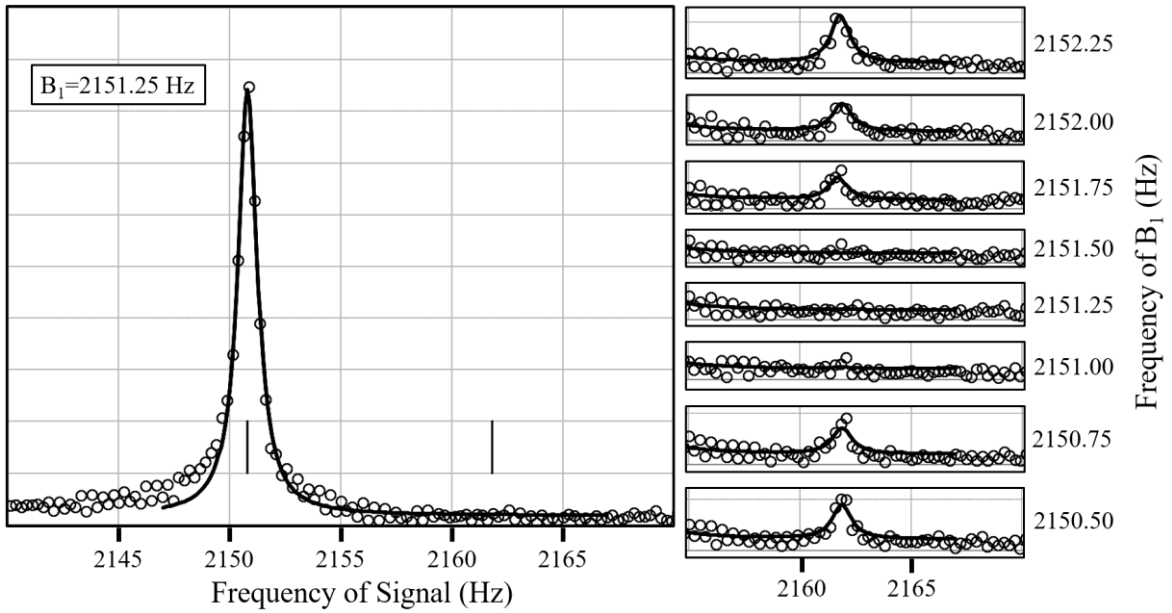

Either of the lines in the ^{1}H spectral doublet could be selected, as in the images below. A pulse at the central frequency excited both lines (though its amplitude had to be increased by about 50% to achieve the π/2 tip angle).

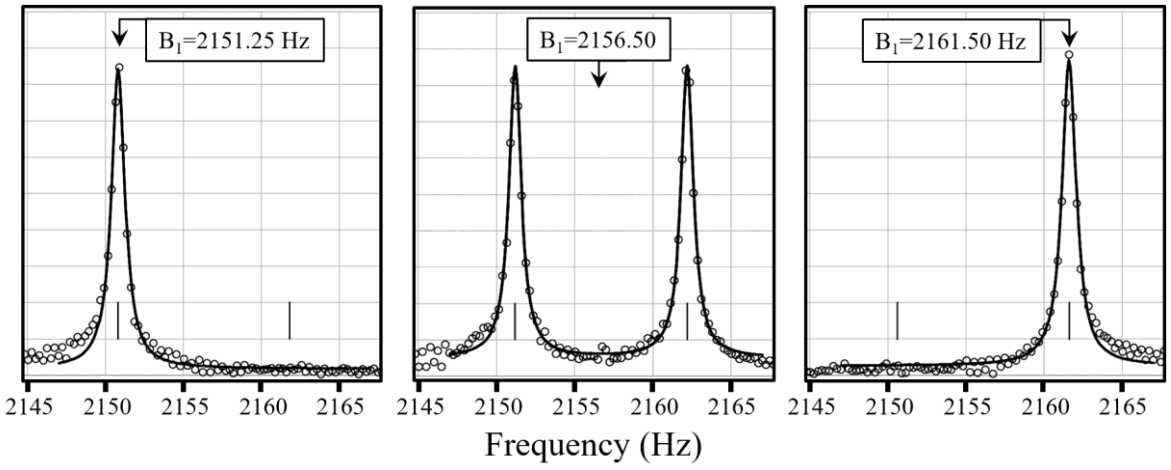

Limitations of the Vector Model of Nuclear Spins

Elementary experiments in 1-dimensional NMR spectroscopy, and even basic Magnetic Resonance Imaging, can be introduced to students with a simple conceptual model in which nuclear spins are visualized as classical vectors in 3 dimensions. In such a model, spins lying initially in the *z*-axis are tipped by $\mathbf{B_1}$ pulses down into the *x*-*y* plane, where the precession of their magnetic moment induces a signal voltage in the receiver coil.

This simple model, however, fails spectacularly when attempting to account for the results of the following experiment.

In the graphs below, a selective $\mathbf{B_1}$ pulse was used to excite only the lower frequency line of the ^{1}H doublet. A π/2 pulse at the ^{31}P frequency then split this single line into a doublet, while a π pulse shifted the line to the higher frequency. The small secondary peak seen with the π pulse indicates the partial loss of coherence.

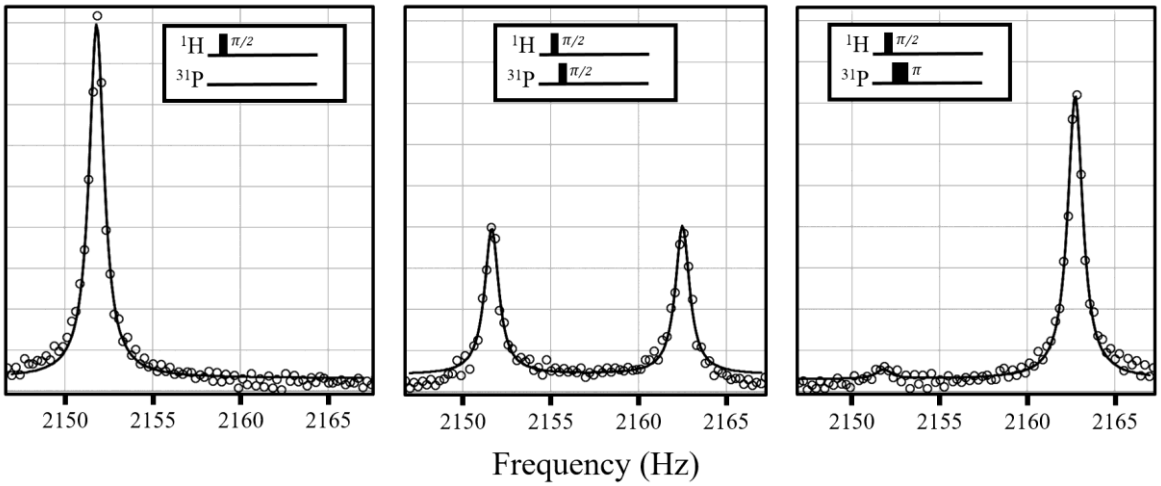

To illustrate the failure of the vector model, let us attempt, as in the images below, to account for this experimental data.

Starting with spin vectors polarized along the *z*-axis (**a**), we applied a selective π/2 $\mathbf{B_1}$ pulse at the ^{1}H frequency, tipping the ^{1}H spins (filled arrow) down into the x-y plane (**b**), where they induced a signal voltage in the receiver coil. So far, so good. We could argue that the selective ^{1}H pulse has affected only that half of the population of TMP molecules whose ^{31}P spins were in the ***up*** spin state (or ***down***, according to our choice of line in the ^{1}H doublet).

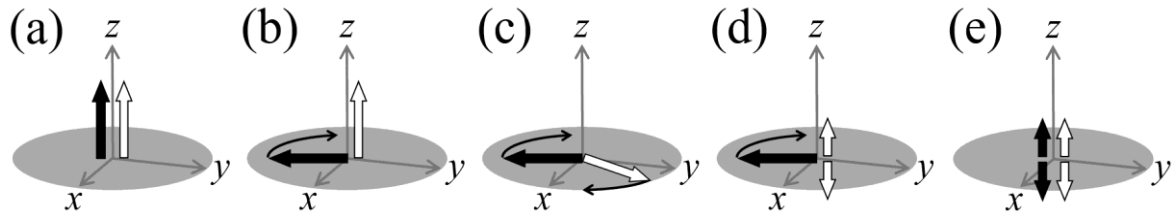

When we applied a π/2 pulse at the ^{31}P frequency, tipping the ^{31}P spins down into the *x*-*y* plane (**c**), the vector model fails. We observed a splitting of the ^{1}H spectrum (image on previous page), yet in classical electrodynamics, there should be no interaction between the two vectors, rotating in the *x*-*y* plane at widely separated frequencies (2,156 and 872 Hz).

We are forced to realize that the ^{31}P spins are not simply tipped down into the *x*-*y* plane, but instead exist as a quantum mechanical superposition of the ***up*** and ***down*** states along the *z*-axis (**d**). In Dirac notation, the effect of the π/2 pulse is: –

$$|up\rangle \xrightarrow{\pi/2} \frac{|up\rangle + |down\rangle}{\sqrt{2}}$$

We might extract the last glimmer from the vector model by proposing that half of the ^{1}H spins were coupled to ^{31}P spins in the ***up*** state and half to spins in the ***down*** state, thus producing the two different frequencies seen in the spectral doublet. But a little more thought will convince us that the ^{1}H spins must, like the ^{31}P, be in a superposition of the ***up*** and ***down*** states (**e**). The minimal model which can cope with the observations is the *Product Operator* formalism, introduced in textbooks (e.g. Keeler, 2011) and widely used in the NMR literature.

Spinor Behavior of Nuclear Spins

We have seen that a π/2 $\mathbf{B_1}$ pulse at the ^{31}P frequency splits the ^{1}H spectral line into a doublet, and a π pulse shifts the ^{1}H signal to a single line at the higher frequency. Further increases in the $\mathbf{B_1}$ pulse energy at the ^{31}P frequency change the ^{1}H spectrum in predictable ways. A 3π/2 pulse results in a doublet ^{1}H signal, while a 2π pulse returns the ^{1}H spectrum to a single line at the lower frequency.

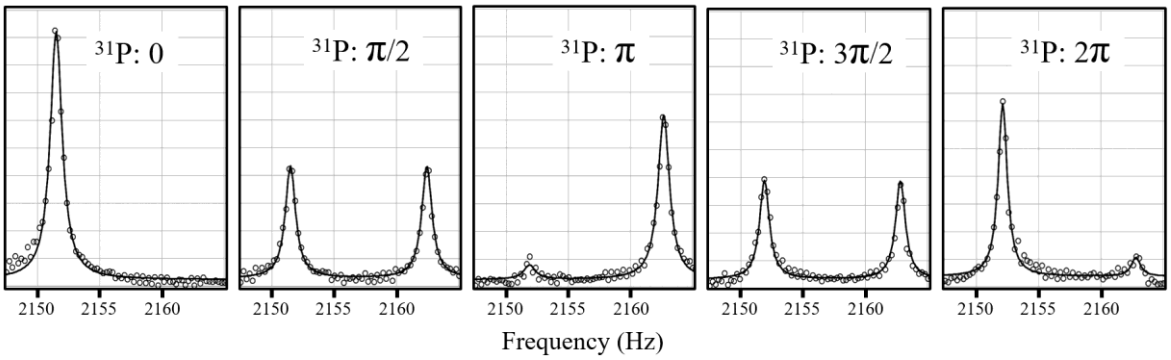

It would seem from the spectra, plotted as absolute magnitudes, that rotating the ^{31}P nuclei by 2π (360 degrees) returns the system to its initial state. Quantum mechanics, however, predicts that spin ½ entities must be rotated 4π (720 degrees) to return to their initial state.

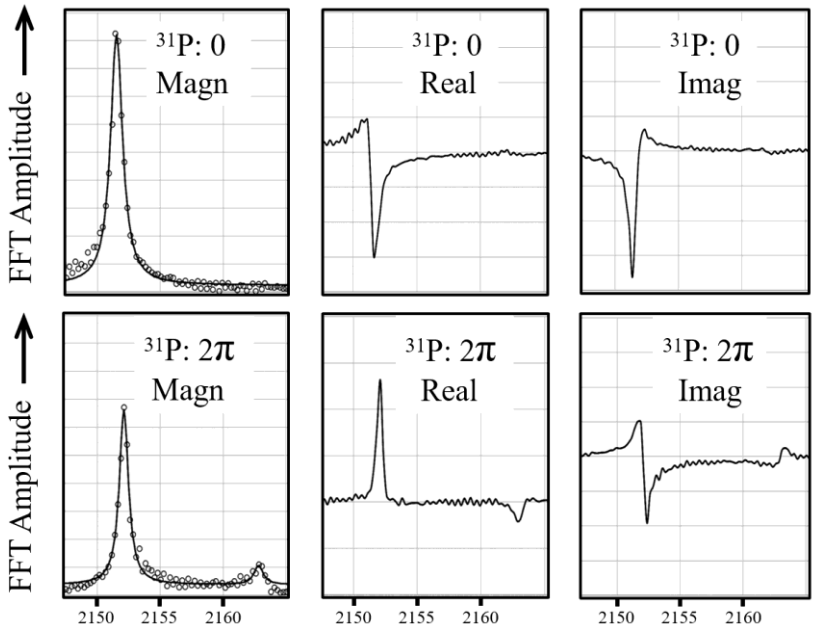

Despite the ^{1}H signals looking comparable when plotted as magnitudes for the zero and 2π rotation of the ^{31}P spins, the real and imaginary components of the Fourier transforms reveal striking differences (images preceding).

This is a manifestation of the spinor behavior of nuclear spins, first demonstrated in NMR by Stoll, Vega & Vaughan (1977), recording a ^{1}H signal while the adjacent ^{13}C spins in formate ions were tipped through 2π in a conventional high-field NMR system. Their report provides a cogent discussion of the principles involved. Interference between the wave functions of two coupled spins reveals wave function phase, usually invisible in NMR of single species, where we observe expectation values of large ensembles. Note that these authors split the ^{13}C doublet with a frequency-selective $\mathbf{B_1}$ pulse, while in the present studies we split the ^{1}H doublet.

As predicted by the quantum mechanics of spinors, a rotation of the ^{31}P spins in TMP through 4π would be required to return the system to its initial state. Unfortunately, due to the loss of coherence with large rotations, a 4π pulse on the ^{31}P spins in our EF-NMR system left too little signal for the data to be convincing.

"EPR State"

Cancellation of the ^{1}H signal was observed following a pair of $\pi/2$ $\mathbf{B_1}$ pulses at the ^{31}P frequency, separated by a time delay of 1/(2J). With careful adjustment of the amplitude and timing of the ^{31}P $\mathbf{B_1}$ pulses, profound suppression of the signal was achievable.

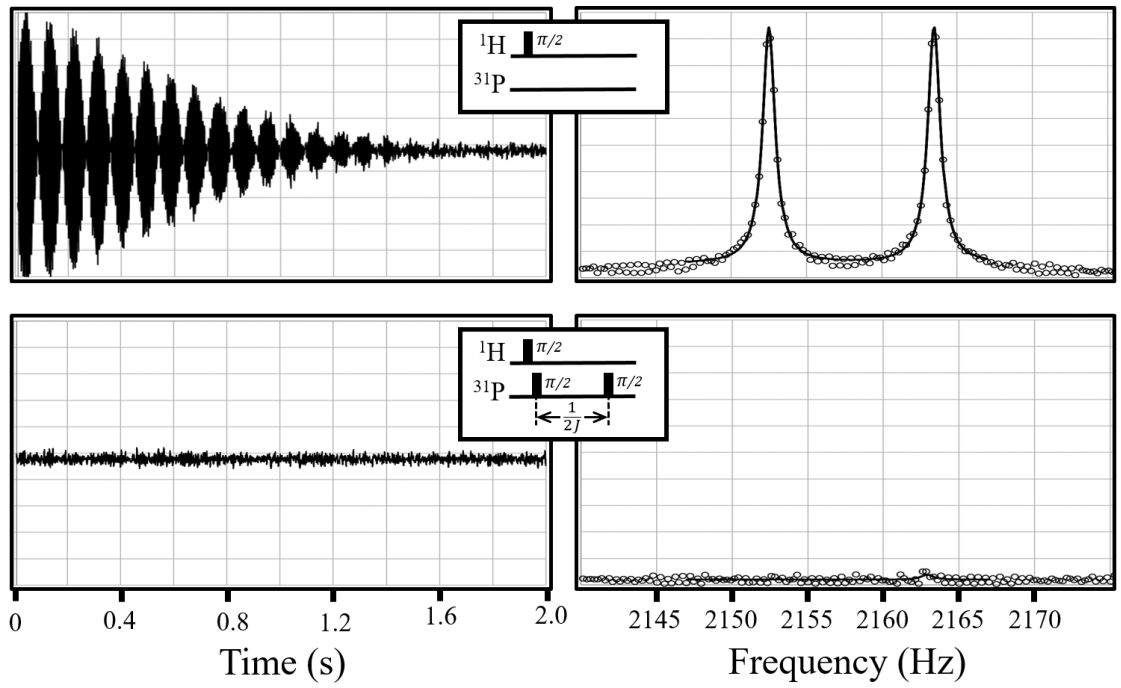

After such a pulse sequence, further $\mathbf{B_1}$ pulses at either the ^{1}H or ^{31}P frequencies failed to evoke a detectable signal. The situation has been described as an *EPR state*, referring to quantum entanglement (e.g. Chuang, Gershenfeld, Kubinec & Leung, 1998: Fig. 6 and discussion). The NMR literature more usually describes such a state as multiple quantum coherence, avoiding the controversial issue of whether any state of an NMR system can justifiably be described as *entangled*. A straightforward explanation can be found in terms of the simple vector model. The first ^{31}P $\pi/2$ pulse splits each ^{1}H spectral line into a frequency doublet. Evolution for a time of 1/(2J) then puts the components of the doublet into opposite phases in the *x*-*y* plane, cancelling the signal. The second ^{31}P $\pi/2$ pulse returns the ^{31}P spins to the *z*-axis, and the ^{1}H spins remain in opposite phases, silent in the receiver channel.

Quantum Computing in NMR

When efforts towards physical implementation of quantum computing began in the late 1990s, it was the mature technology of high-field NMR which provided easy access to small-scale model systems (Jones, 2001). This work was inspired by Lloyd (1993), who proposed using adjacent nuclear spins in molecules as arrays of weakly-coupled quantum entities that could be manipulated by electromagnetic pulses of controlled energy and time: the $\mathbf{B_1}$ pulses of conventional NMR.

The techniques for practical realization of NMR quantum computing were presented in overview by Gershenfeld & Chuang (1997) in the journal ***Science***, and discussed in detail in ***Proceedings of the Royal Society*** (Chuang, Gershenfeld, Kubinec & Leung, 1998).

Although of severely limited scalability, such NMR systems were able to validate important theoretical principles. Fast searching using the Grover algorithm was demonstrated in a toy system of 2 qubits (4 states) using ^{13}C-enriched chloroform (Chuang, Gershenfeld & Kubinec, 1998). A popular account appeared in ***Scientific American*** (Gershenfeld & Chuang, 1998).

Shor's algorithm, which finds the prime factors of a number, *N*, in a time which is polynomial rather than exponential in *N*, was used on a 7-qubit system (5 ^{19}F and 2 ^{13}C spins in perfluorobutadiene) to factorize the number 15 (Vandersypen *et al*., 2001). A 12-qubit system has been demonstrated (Lu *et al*, 2017).

In a domain replete with counter-intuitive phenomena, one of the most striking deductions of quantum mechanics is the No-Hiding Theorem (Braunstein & Pati, 2007). Although coherence is readily lost from quantum systems interacting with a hot environment, No-Hiding dictates that their information cannot be destroyed, but instead must move into environmental degrees of freedom uncorrelated with the system. Experimental confirmation of this powerful theoretical insight was achieved in a 3-qubit NMR system (^{13}C-enriched $CHFBr_2$) by Samal, Pati & Kumar (2011).

High-field NMR involves precession frequencies of hundreds of MHz and $\mathbf{B_1}$ pulse widths of microseconds. Complex pulse sequences can readily be accommodated, granted the persistence of transverse magnetization for times (T_2) of the order of a second. In EF-NMR, the low precession frequency, around 2 kHz, dictates $\mathbf{B_1}$ pulse widths of tens of milliseconds, limiting experimental protocols to only a few pulses.

Despite this limitation, EF-NMR can demonstrate an important principle of NMR quantum computing: the interaction of two spins through J-coupling such that the relationship between the input and output states of one spin can be controlled by the state of the other. In particular, the operation of a quantum C-NOT gate can be demonstrated.

To read a qubit represented by a spin in the ***up*** (0) or ***down*** (1) state, a $\pi/2$ $\mathbf{B_1}$ pulse is applied to tip the spin into the *x*-*y* plane, the phase of the readout signal revealing the state.

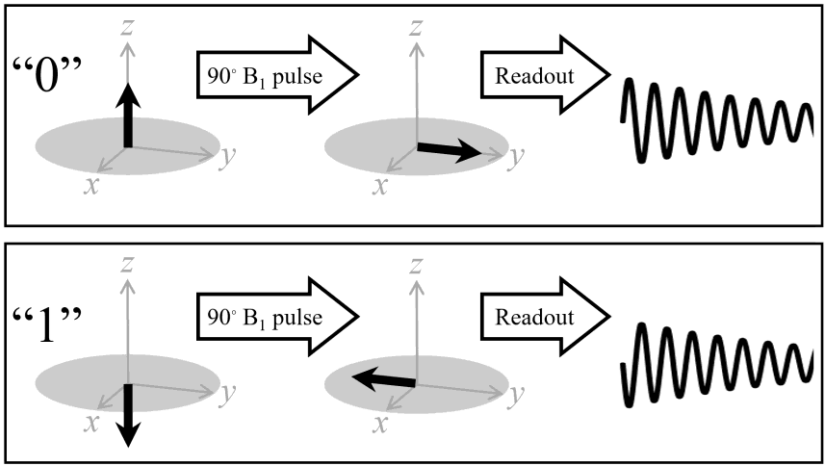

The vector model is adequate for an introductory presentation. The phase of an NMR signal is easily demonstrated, for teaching purposes, by displaying the first few cycles of the acquired data in the voltage-time domain. In the figure following, the signal (open circles) was modelled (solid line) with a sinewave function, $sin(2\pi ft+\varphi)$, where f is frequency and φ is phase, the model being optimized by least squares. The phase shift was 182 degrees, close to the ideal value of 180 degrees (π).

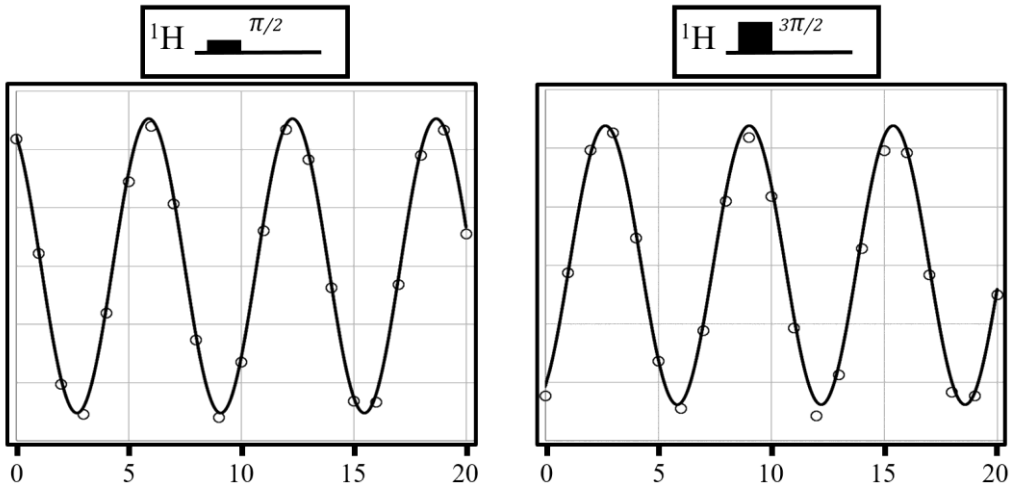

Quantum computing logic functions are implemented in NMR using the J-coupling interaction between the spins representing qubits.

The state of a spin at the end of a pulse sequence may depend on the state of a second nucleus, whose effect on the spin's precession frequency influences the phase of its spin vector before a final $\mathbf{B_1}$ pulse tips it back into the ***up*** or ***down*** state.

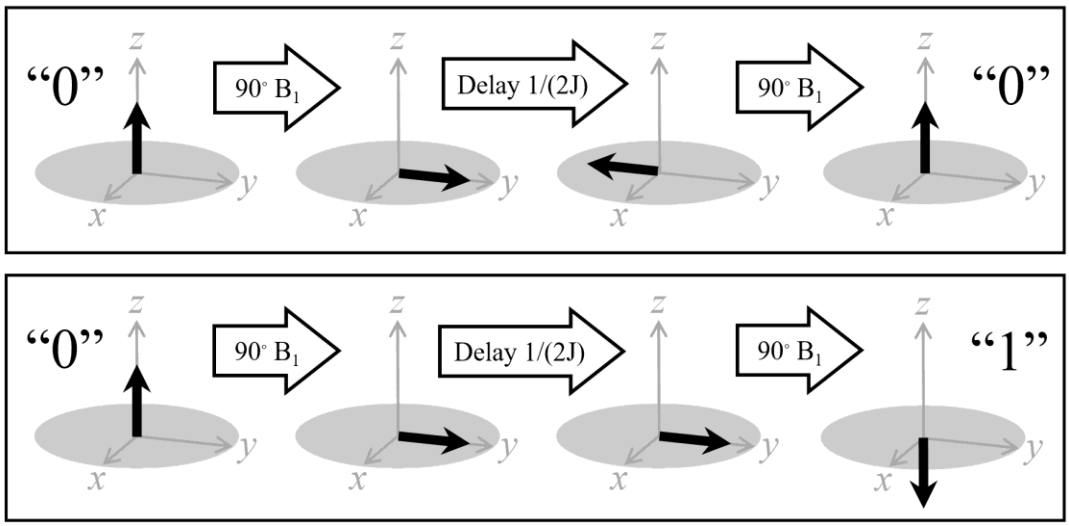

In our example with ^{1}H and ^{31}P, the state of the ^{31}P spin (***up*** or ***down***) alters the ^{1}H precession frequency by J = 11 Hz. A delay of $1/(2J)$ results in the phase of the ^{1}H spin vector differing by 180 degrees between the situation with ^{31}P ***up*** and ^{31}P ***down***. Thus, when the final 90 degree $\mathbf{B_1}$ pulse tips the ^{1}H spin back into the z-axis, the ^{1}H spin may return to its initial state (0→0, 1→1) or be flipped to its complement (0→1, 1→0), according to the state of the ^{31}P spin.

These conversions of logic states are analogous to the Exclusive-OR (XOR) function implemented in silicon chip logic gates (e.g. the 7486), where the state of inputs A and B determine the state of the Output (with 0 being represented by a low voltage and 1 by a high voltage).

A	B	Output
0	0	0
0	1	1
1	0	1
1	1	0

In quantum computing, A and B are the state of spins, and as well as converting input A to an Output, we preserve input B. The result is a gate with two inputs and two outputs, known as Controlled-NOT, or C-NOT. The state of input B (in our case the ^{31}P spin) determines whether the spin representing input A (^{1}H) will be flipped or left unchanged.

To present an EF-NMR experiment demonstrating the C-NOT gate to students requires some preliminary explanation.

We first consider a theoretical scheme as outlined in the diagram below. It is divided into three phases: preparation of the input states for the gate, the C-NOT gate itself, and the readout of the signal whose phase encodes the output state of the gate. With 7 $\mathbf{B_1}$ pulses, this scheme would be challenging to implement in EF-NMR, decay of the transverse magnetization during the extended time-course causing signal degradation. As we shall see, a simplified scheme with fewer $\mathbf{B_1}$ pulses is able to illustrate the function of the C-NOT logic gate and is practicable in EF-NMR. The full 7-pulse sequence in the diagram below, however, provides conceptual clarity for an introductory presentation.

At time marked **(a)** in the diagram below, the polarizing field has been applied, and we are ready to commence the $\mathbf{B_1}$ pulse sequence. The first $\mathbf{B_1}$ pulse is frequency-selective (soft) and tips the ^{1}H spins $\pi/2$. Note that this pulse selects that half of the total population of TMP molecules whose ^{31}P spin orientation, ***up*** or ***down***, corresponds with the frequency of the ^{1}H precession selected by the $\mathbf{B_1}$ pulse. The ^{1}H spins are now in the *x*-*y* plane of the vector model.

To prepare the ^{1}H spins in the ***up*** or ***down*** state requires another $\pi/2$ pulse to tip the spins back into the *z*-axis. We select whether the ^{1}H spins will be ***up*** or ***down*** by applying (or not applying) a π (180˚) pulse before the $\pi/2$ pulse.

The state of the ^{31}P spins, ***up*** or ***down***, was selected initially by the choice of frequency for the soft ^{1}H pulse which began the sequence. The ^{31}P spins may be tipped to the opposite state by a π pulse at the ^{31}P precession frequency.

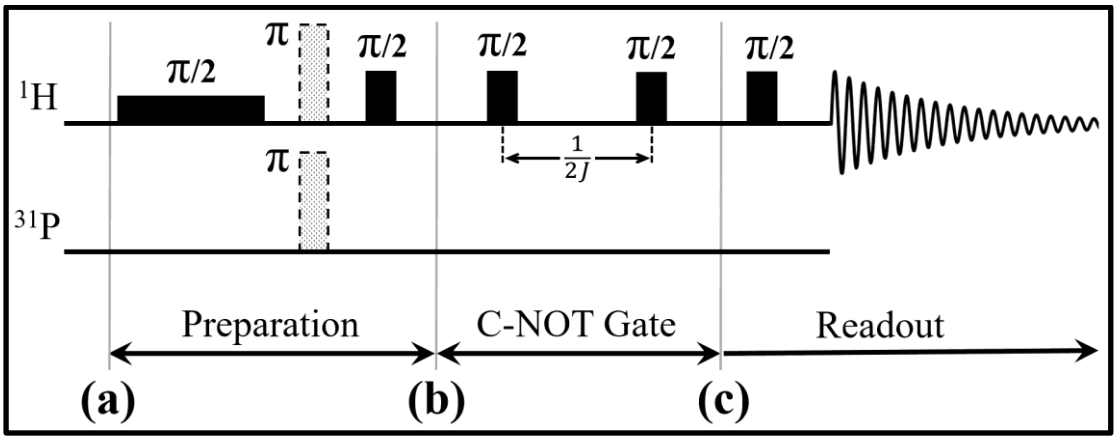

At the end of the Preparation phase, the point marked **(b)** in the diagram above, we have the ^{1}H and ^{31}P spins in the *z*-axis, in a state, ***up*** or ***down***, determined by the presence or absence of π pulses at the corresponding frequencies. Thus by the appropriate choice of pulses, we can prepare all 4 combinations of input states for the C-NOT gate.

The gate function is then implemented by tipping the ^{1}H spins down into the *x*-*y* plane with a $\pi/2$ pulse. They will be allowed to precess for a time $1/(2J)$, resulting in their

magnetization vector being orientated along the **+*y*** or **–*y*** axis, according to their precession frequency, which depends on the state of the ^{31}P spins. A second π/2 pulse then tips the ^{1}H spins back into the *z*-axis, orientated ***up*** or ***down*** according to their previous state in the *y*-axis. This is the output state of our quantum logic gate at point marked **(c)** in the diagram.

To generate a readout signal, we apply a π/2 pulse at the ^{1}H frequency. The phase of the signal encodes the state of the ^{1}H spins.

Although conceptually straightforward, the scheme outlined above would be difficult to implement in EF-NMR. It is also unnecessarily complex, if the aim is simply to demonstrate the principle of the C-NOT gate. We notice that point **(b)** separates two π/2 pulses, and point **(c)** also separates two π/2 pulses. Such pairs of π/2 pulses invert the spin vector, **+z** → **–z**, and **–z** → **+z**. The four pulses cause a total rotation of 2π (360°), without visible effect on the phase of the readout.

For demonstration purposes, we can omit these four π/2 pulses, provided we preserve the 1/(2*J*) time interval before acquisition of the signal. The π/2 and optional π pulses at the ^{1}H frequency can be combined into a single selective pulse whose amplitude is set to provide the desired tip angle. The simplified pulse sequence is easy to implement in EF-NMR and demonstrates the essential mechanism of the C-NOT gate: the change in phase of the ^{1}H spins during the delay time of 1/(2*J*), depending on the state of the ^{31}P spins.

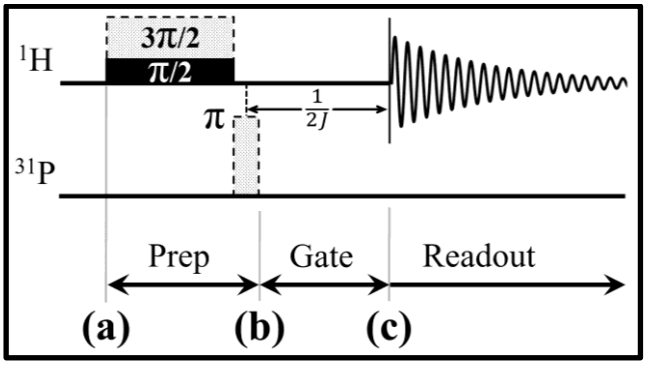

The 4 different input states to the gate are selected by the amplitude of the soft ^{1}H pulse and by the presence or absence of the hard π pulse at the ^{31}P frequency.

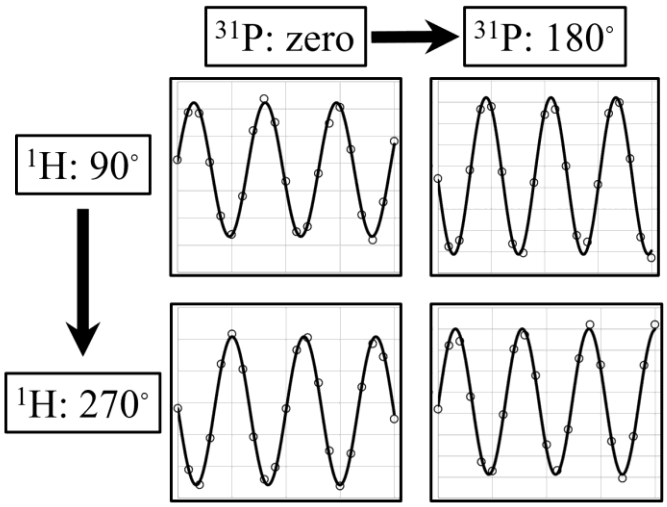

As we see in the graphs above, the first few cycles of the readout revealed the phase of the ^{1}H signal, which was reversed if a π pulse tipped the ^{31}P spins.

The shifts in phase, measured by least-squares fitting of a sinusoidal function to the data samples, are shown in the table following (units: degrees).

	^{31}P: 0°	^{31}P: 180°
^{1}H: 90°	0	176
^{1}H: 270°	171	-10

The values were within 10 degrees of the ideal 0 and 180 values.

Thus we have demonstrated the principle of the quantum computing C-NOT gate. By inverting the spin vector of the ^{31}P nuclei with a π/2 $\mathbf{B_1}$ pulse, we inverted the phase of the ^{1}H spins which generated the readout signal. A further π/2 $\mathbf{B_1}$ pulse at the ^{1}H frequency would tip the ^{1}H spins back into the *z*-axis, in the ***up*** or ***down*** state, which could be the desired situation for further manipulation, but of course would give no readout signal.

Conclusions

Trimethyl phosphate provides a convenient heteronuclear system for illustrative experiments in EF-NMR. While only the ^{1}H signal is readily acquired, both the ^{1}H and ^{31}P nuclear spins can be manipulated independently by $\mathbf{B_1}$ pulses.

J-coupling splits the ^{1}H signal into a well-resolved doublet, and a soft $\mathbf{B_1}$ pulse of duration 1/*J* with carefully-adjusted frequency will isolate a single line of the doublet. A hard π/2 pulse at the ^{31}P frequency will then split the ^{1}H line into a doublet, while a π pulse moves it to a single line at the alternate frequency. This behavior reveals the failure of the intuitive model representing nuclear spins as classical vectors, compelling students to realize that spins tipped into the *x-y* plane by a π/2 $\mathbf{B_1}$ pulse are actually a quantum-mechanical superposition of the ***up*** and ***down*** states along the *z*-axis.

Quantum mechanical spinor behavior is revealed by examining the real and imaginary components of the ^{1}H readout signal after a 2π rotation of the ^{31}P spin.

The principle of a quantum computing C-NOT gate can be illustrated by allowing the ^{1}H spin to precess for a time 1/(2*J*) before readout, thus inverting or not inverting its state, according to the state of the ^{31}P spin. All 4 input states of the gate can be prepared by a selective ^{1}H $\mathbf{B_1}$ pulse of π/2 or 3π/2 tip angle followed by an optional hard ^{31}P pulse of π tip angle.

References

Braunstein, S.L. & Pati, A.K. (2007). *Quantum Information Cannot Be Completely Hidden in Correlations: Implications for the Black-Hole Information Paradox*. ***Physical Review Letters* 98**, 080502. Preprint: ***arXiv:gr-qc***/0603046.

Callaghan, P.T., Eccles, C.D. & Seymour, J.D. (1997). *An earth's field nuclear magnetic resonance apparatus suitable for pulsed gradient spin echo measurements of self-diffusion under Antarctic conditions*. ***Review of Scientific Instruments* 68**, 4263. The equipment was developed and marketed by Magritek (NZ) as the *Terranova-MRI* from 2004. Demonstration videos online at: *https://magritek.com/resources/videos/* (retrieved Sept 26, 2020).

Chuang, I.L., Gershenfeld, N. & Kubinec, M. (1998). *Experimental Implementation of Fast Quantum Searching*. ***Physical Review Letters* 80**, 3408-3411.

Chuang, I. L., Gershenfeld, N., Kubinec M. G. & Leung, D. W. (1998). *Bulk quantum computation with nuclear magnetic resonance: theory and experiment*. ***Proceedings of the Royal Society of London A* 454**, 447-467.

Gershenfeld, N.A. & Chuang, I.L. (1997). *Bulk Spin-Resonance Quantum Computation*. ***Science* 275**, 350-356.

Gershenfeld, N. & Chuang, I.L. (1998). *Quantum Computing with Molecules*. ***Scientific American***, issue of June 1998.

Jones, J.A. (2001). *Quantum Computing and Nuclear Magnetic Resonance*. ***Physical and Chemical Communications* 4**, 49-56. Preprint: ***arXiv:quant-ph***/0106067.

Keeler, J. (2010). *Understanding NMR Spectroscopy*. Wiley, ISBN: 978-047074609 Amazon Kindle (2011), ASIN : B005UQCYBC.

Lloyd, S. (1993). *A Potentially Realizable Quantum Computer*. ***Science* 261**, 1569-1571.

Lu, D., Li, K., Li, J., Katiyar, H., Park, A.J., Feng, G., Xin, T., Li, H., Long, G., Brodutch, A., Baugh, J., Zeng, B. & Laflamme, R. (2017). *Enhancing quantum control by bootstrapping a quantum processor of 12 qubits*. ***npj Quantum Information* 3**, 45 (7 pp).

Mann, P.B., Clark, S., Cahill, S.T., Campbell, C.D., Harris, M.T., Hibble, S., To, T., Worrall, A. & Stewart, M. (2019). *Implementation of Earth's Field NMR Spectroscopy in an Undergraduate Chemistry Laboratory*. ***Journal of Chemical Education* 96**, (10), 2326-2332.

Michal, C.A. (2010). *A low-cost spectrometer for NMR measurements in the earth's magnetic field*. ***Measurement Science and Technology* 21**, 1-9.

Robinson, J.N., Coy, A., Dykstra, R., Eccles, C.D., Hunter, M.W. & Callaghan, P.T. (2006). *Two-dimensional NMR spectroscopy in Earth's magnetic field*. ***Journal of Magnetic Resonance* 182**, 343-347.

Samal, J.R., Pati, A.K. & Kumar, A. (2011). *Experimental Test of the Quantum No-Hiding Theorem*. ***Physical Review Letters* 106**, 080401. Preprint: ***arXiv:***1004.5073 [quant-ph]

Stoll, M.E., Vega, A.J. & Vaughan, R.W. (1977). *Explicit Demonstration of Spinor Character for a Spin ½ Nucleus via NMR Interferometry*. ***Physical Review A* 16**, 1521-1525.

Teachspin Inc., 2495 Main Street, Buffalo, New York 14214. Details online at: https://www.teachspin.com/earths-field-nmr

Trevelyan. (2019). *MRI and NMR Spectroscopy in the Earth's Field: Building a Low-Cost NMR Spectrometer for Hobby Science and Teaching*. ***Amazon*** ISBN-10: 109378539X, also ***Amazon Kindle*** ASIN: B07QNSLZCS.

Vandersypen, L.M.K, Steffen, M., Breyta, G., Yannoni, C.S., Sherwood, M.H. & Chuang, I.L. (2001). *Experimental realization of Shor's quantum factoring algorithm using nuclear magnetic resonance*. ***Nature* 414**, 883–887. Preprint: ***arXiv:quant-ph***/0112176

Appendix: Technical Notes

Shielding the coil assembly with a concentric metal screen improves the signal-to-noise ratio of EF-NMR equipment in typical laboratory environments. High-order harmonics of the power mains frequency are generated by switching transients in the power supply circuitry of appliances (e.g. 43 x 50 = 2150 Hz, 35 x 60 = 2100 Hz). At the low frequency of the power mains, the skin depth in metal conductors is of the order of millimeters, and a shield thickness several times the skin depth is necessary for effective screening. In the

studies reported, a cylindrical shield of aluminium, 15 mm thick, 450 mm long and with an internal diameter of 150mm, was found to be effective is suppressing interference from the power mains. If aluminium tubing with 15 mm wall thickness proves difficult to source, a work-around is to wrap 10 kg of the inexpensive aluminium flashing used in roof construction around a former.

Coil design in EF-NMR is dictated by function. The 3 functions of the coils are (1) applying the pre-polarization field, (2) applying the $\mathbf{B_1}$ field in pulses and (3) acquiring the signal by Faraday induction from the precession of the magnetic moments of the nuclear spins. Combining these functions in a single coil is seldom attempted, functions (1) and (3) being highly incompatible.

The signal receiver coil in the reported studies was 4,000 turns of 0.25 mm enameled copper wire, wound in 10 layers of 400 turns each, on a length of 80 mm plastic DWV pipe sourced from a building supply retailer. The layers were separated by PVC adhesive tape 0.15 mm thick. The coil's resistance was 317 Ω and its free-air inductance was 566 mH, falling to 376 mH in its final position inside the polarization coil and aluminium shield. It was brought to resonance at the signal frequency of 2.156 kHz with a parallel capacitance of 12 nF, in addition to the internal capacitance of the coil itself and the capacitance of 3 meters of coaxial cable connecting to the amplifier.

A specimen cassette, 100 mm long and constructed from 65 mm DVW pipe with end caps, held 300 ml of water, or other fluids compatible with plastics, such as alcohols, oils or aqueous solutions. A 500 ml glass stock bottle of TMP, originally from Tokyo Chemical Industries and available from several scientific supply retailers, fitted snugly inside the 80 mm former of the receiver coil. The use of unopened reagent bottles has advantages for safety in a classroom environment.

For maintenance of spin coherence in studies such as those reported here, uniform tip angles throughout the specimen are required: a highly uniform $\mathbf{B_1}$ field must be achieved. The simplest coil geometry delivering a uniform magnetic field is a long solenoid.

A coil of 1,425 turns of 1.5 mm enameled copper wire in 6 layers was wound on a 110 mm former of plastic DWV pipe, with the first layer being 240 turns (360 mm long) and successive layers wound in the grooves of the layer below. The layers were terminated individually and connected in series by connectors running longitudinally, outside the windings. To improve the uniformity of the magnetic field in the specimen zone at the center of the coil, small correction coils of 47 turns were wound over the ends of the windings and connected electrically in series. Calculation suggests that uniformity across the central 100 mm of such a coil would be better than 1 part per 1,000. In practice, however, variation in the pitch of the windings proved to be the limiting factor.

The coil weighed circa 10 kg, had a resistance of 5 Ω, and an inductance in free air of 66 mH, falling to 22 mH inside the aluminium shield. It was used both for pre-polarization, with 5 A current producing a central field of 25 mT, and for $\mathbf{B_1}$ injection, where it presented an inductive load to the driving circuitry of around 300 Ω at the ^{1}H frequency and 120 Ω at the ^{31}P frequency. With its large surface area, the coil remained safely below the temperature limit for DVW pipe (70° C) while driven 6 seconds on, 12 seconds off (for $\mathbf{B_1}$ sequence, signal acquisition and decay of polarization) during experiments of several hours duration. Large eddy currents were induced in the aluminium shield by the current quench at the end of the pre-polarization period, and a delay of 200 milliseconds was needed for the $\mathbf{B_0}$ field to settle to its natural value, as assessed by the ^{1}H precession frequency.

Convenient electronic circuitry for switching the pre-polarization and $\mathbf{B_1}$ pulse currents under control of an Arduino microcontroller has been described (Trevelyan, 2019).

Signal amplification is straightforward, only the first amplifier stage being critical. A voltage noise amplitude well below 1 μV at bandwidth-limited signal frequencies is essential, mandating a specialized low-noise op-amp with a noise figure around 1 nV/√Hz. The Linear Technologies LT1028 device was used in a non-inverting configuration with voltage gain of ×100. It is available in traditional 8-pin DIP, much easier to handle in a prototyping situation than the surface mount packages ubiquitous in commercial manufacture. Following stages, using conventional audio techniques, provided a further gain of ×1000 and restriction of bandwidth to 200 Hz, yielding signal levels convenient for the low-cost DSOs usually found in student laboratories, or for A-D conversion with direct acquisition into the computer.

In outdoor environments, the Earth's magnetic field, which we are using as $\mathbf{B_0}$, typically shows excellent uniformity, giving FID signals of seconds duration and yielding spectral linewidths of less than 1 Hz. The field in the laboratory, however, may be distorted by ferromagnetic metals in equipment and building structures. Selection of an optimum placement for the coil unit by trial and error can minimize the effect, but often not eliminate it. A first-order shimming system, with large coils wired as opposing pairs in 3 axes, can substantially improve field uniformity (Trevelyan, 2019).

Adjustment of shim currents is laborious, but if the coil unit and its surroundings are left undisturbed, need be done only once. Rough settings can be found by visual inspection of the FID in real time, and fine adjustments made by examination of the line width, assessed as the γ parameter of absorption-mode Lorentzian functions fitted by least squares. The graph below shows the fine-tuning of one of the axes of the shim system when it was close to optimal.